Smoothing of transverse nonuniformities at the critical density in laser interaction with nonuniform plasmas

Dimitri Batani[1] , Vasyl Maslov[2], Denis Bondar[2], Elvira Bilokon[2] and Valeria Bilokon[2]

[1]CELIA, University of Bordeaux, Bordeaux, France and [2]Karazin Kharkiv National University, Kharkiv, Ukraine

Abstract

This study addresses the smoothing of transverse inhomogeneities at the critical layer for S- and P-polarized laser pulses interacting with plasmas which are inhomogeneous in the pulse propagation direction. Numerical simulations, incorporating ion mobility, demonstrate the formation of low-density plasma channels, which serve as waveguides for the lower-frequency components of the laser pulse. These channels are enclosed by regions of higher plasma electron density that act as scattering mirrors for the higher-frequency components. The channels are inclined relative to the direction of laser propagation. At the critical layer, where the pulse amplitude intensifies, localized plasma electron cavities initially form before merging into a uniform transverse channel due to the ponderomotive force of the trapped electromagnetic field. These findings are relevant to inertial confinement fusion, as they suggest that the homogenization of plasma structures could facilitate more uniform energy deposition in the supercritical plasma region and the shock-wave formation area.

Introduction

The development of instabilities and localized inhomogeneities is a well-known phenomenon in laser–plasma interactions. These include short solitary perturbations (1–5), cavitons containing trapped Langmuir waves (5–7), and shock wave formation (8,9). While such effects are of fundamental interest, they pose challenges for inertial confinement fusion (ICF), where uniform energy deposition is essential. This is particularly critical in the context of direct-drive and shock ignition approaches (10–16). Despite their importance, the physical mechanisms underlying the smoothing of inhomogeneities remain not fully understood; ponderomotive forces and hot electron pressure are believed to play significant roles.

In this study, we examine plasma with a longitudinally varying electron density, increasing up to twice the critical density for the incident laser radiation. Using numerical simulations, we investigate the self-consistent smoothing of transverse inhomogeneities near the critical layer (where $n_e \approx n_e (x_{cr}) = n_{cr}$) for both S- and P-polarized laser pulses. Initially, small-scale transverse modulations form at the leading edge of the laser pulse. These structures subsequently evolve into a single, uniform transverse channel. Our results indicate that, for laser pulses propagating in inhomogeneous plasmas, transverse inhomogeneities are naturally suppressed near the critical layer ($x = x_{cr}$).

Simulations reveal the formation of channels with reduced electron density, oriented obliquely relative to the laser propagation axis – resembling the structures observed in relativistic laser–plasma interactions (17–19). The laser pulse is modeled with finite spectral width. In this context, the low-density regions act as waveguides for lower-frequency components, steering them toward the critical density surface. Surrounding higher-density regions, in turn, scatter the higher-frequency components. At the end of these channels, cavities of reduced electron density form and trap portions of the laser field, locally enhancing its amplitude. Over time, these structures merge to form a continuous transverse channel due to the combined influence of ponderomotive forces, plasma pressure gradients, and wave scattering.

The primary goal of this work is to demonstrate, via simulations, the self-consistent transformation of initial transverse modulations into a uniform transverse channel near the critical density surface, with explicit consideration of ion mobility. Our findings suggest that this mechanism facilitates laser energy homogenization – an essential condition for efficient energy coupling in inertial confinement fusion.
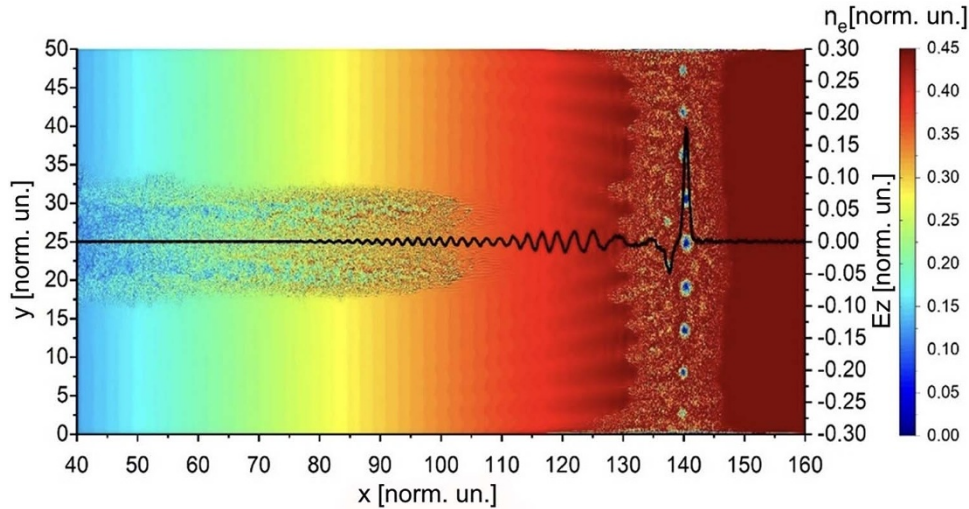
Figure 1. Spatial distribution of plasma electron density $n_e(x, y)$ (shown by colors) and of the laser pulse field E_z (shown by black line) at time $t = 500$. The plasma is initially inhomogeneous along the x direction with density growing linearly from zero to a maximum value $n_{e,max} = 2n_{cr}$. The critical density layer in the graphs is at $x = x_{cr} = 140$.

Simulation setup

We consider a two-dimensional (2D) model to describe the interaction of a laser pulse with an inhomogeneous plasma. In this configuration, the **longitudinal direction (x)** corresponds to both the plasma density gradient and the direction of laser propagation, while the **transverse direction (y)** accounts for plasma inhomogeneities across the beam profile. The plasma electron density increases linearly along the x-axis from zero up to a maximum value of $n_{e,max} = 2n_{cr}$, where n_{cr} is the critical plasma density for the incident laser radiation.

The laser pulse is modeled using an envelope approximation. Longitudinally, it is represented by a function resembling a Gaussian profile ($\cos^2\left[\kappa_\ell\left(x - V_g t\right)\right] = 0.5\left[1 + \cos\left[2\kappa_\ell\left(x - V_g t\right)\right]\right]$) centered around its group velocity V_g and characterized by a pulse length $l = 2\pi/k_l$. In the transverse direction (y), the laser has a Gaussian intensity profile with an initial full width at half maximum (FWHM) of 2λ. The duration at half maximum of the laser pulse equals $100\,\pi/\omega_0$. Therefore, for $\lambda = 438$nm the width of the laser beam is $\approx 1\mu m$, the length of the laser pulse is $\ell \approx 22\mu m$ and its duration $\tau = \ell/c = 2\pi/c\kappa_\ell$ is approximately $\tau = 73fs$. The laser intensity is selected to match values used in previous studies (14, 19), ensuring compatibility with established experimental and simulation conditions.

We separately considered the two cases of S-polarization (E_z, B_y) and P-polarization (E_y, B_z). The normalized amplitude of the laser pulse is $a_0 = eE_{z0}/(m_e c\omega_0) = 0.034$ in the case of S-polarized pulse and $a_0 = eE_{y0}/(m_e c\omega_0) = 0.034$ in the case of P-polarized pulse. Simulations are performed using the fully relativistic particle–in–cell code UMKA 2D3V. The computational domain (x, y) is a rectangular box: $0 < x < L = 300\lambda$ in the longitudinal direction and $0 < y < 50\lambda$ in the transversal direction, where λ is the laser wavelength in vacuum (this means $x < 130\mu m$ and $y < 22\mu m$ in physical units). The laser pulse enters the computation region from the left boundary where $n_e = 0$ and it is incident normally on the plasma (i.e. propagating along x). Ions are mobile and an ion to electron mass ratio $M/m = 25$ is used in the simulations.

The computational time step is $\tau = 0.05\,t_0$, where $t_0 = 2\pi/\omega_0$ is the laser period, the number of particles per cell is 8 and the total number of particles is 15.96×10^6. The simulations presented in this paper were carried out up to 800 laser periods. In the results, the coordinates x and y, time t, electric field amplitude E_{z0} and E_{y0}, and electron plasma density n_0 are given in units of λ, t_0, $m_e c\omega_0/(2\pi e)$, and $2n_{cr}$.

Periodic boundary conditions are applied to the electromagnetic field in the transverse direction (along y). This setup enables the study of the interaction between a laser beam with a large focal spot and the plasma, where the beam is modulated over a transverse distance of 50λ, effectively modeling a comb-like structure of laser filaments injected longitudinally – an approach relevant to inertial confinement fusion (ICF). For example, this configuration can represent a laser beam with an overall transverse envelope of approximately 500μm, as commonly used in laser–plasma interaction experiments, with a modulation period of 22μm. This is equivalent to injecting a bundle of about 23 laser filaments, each with a transverse dimension of ~1μm, into the plasma.

The simulation results show that despite the initial modulation, the energy deposition within the computational domain becomes uniform. This indicates that transverse nonuniformities in a larger laser beam can be effectively smoothed out over propagation distances on the order of 50λ. Such smoothing is particularly significant for practical applications in the context of ICF, especially for the shock ignition scheme, where uniform energy delivery is essential for efficient target compression and ignition.

Results of simulations

Case of S-polarized laser light

At first, we consider the case of S-polarized laser pulse with intensity $I \approx 10^{16} W/cm^2$ and normalized amplitude 0.034. Figures 1–3 show the spatial distribution of the plasma electron density $n_e(x, y)$ and the value of the electric field components $E_z(x)$, $E_x(x)$, $E_y(x)$ at time $t = 500$ (here E_z is the laser pulse electric field). The critical density $n_{cr} = n_e(x_{cr})$ is located at the position
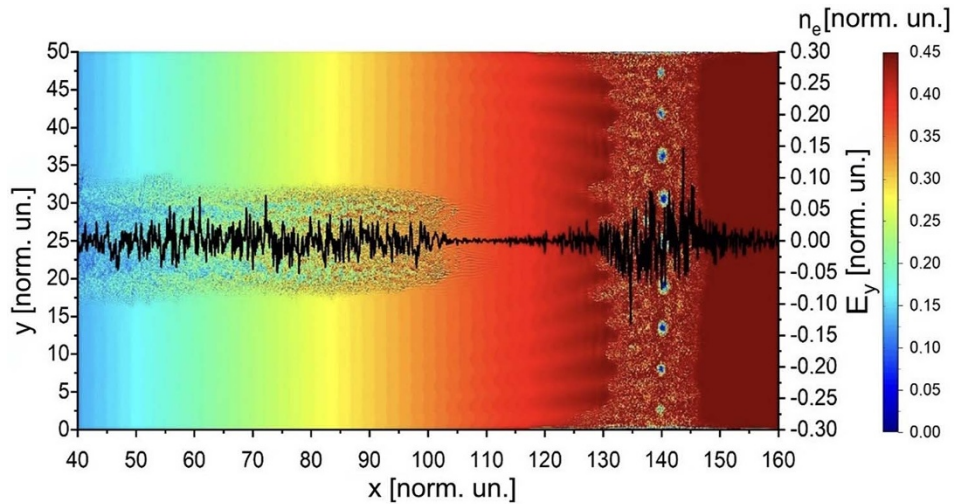
Figure 2. Spatial distribution of plasma electron density $n_e(x,y)$ (shown by colors) and the distribution of field $E_y(x)$ (shown by black line) at time $t = 500$.

Figure 3. Spatial distribution of plasma electron density $n_e(x,y)$ (shown by colors) and the distribution of field $E_x(x)$ (shown by black line) at time $t = 500$.

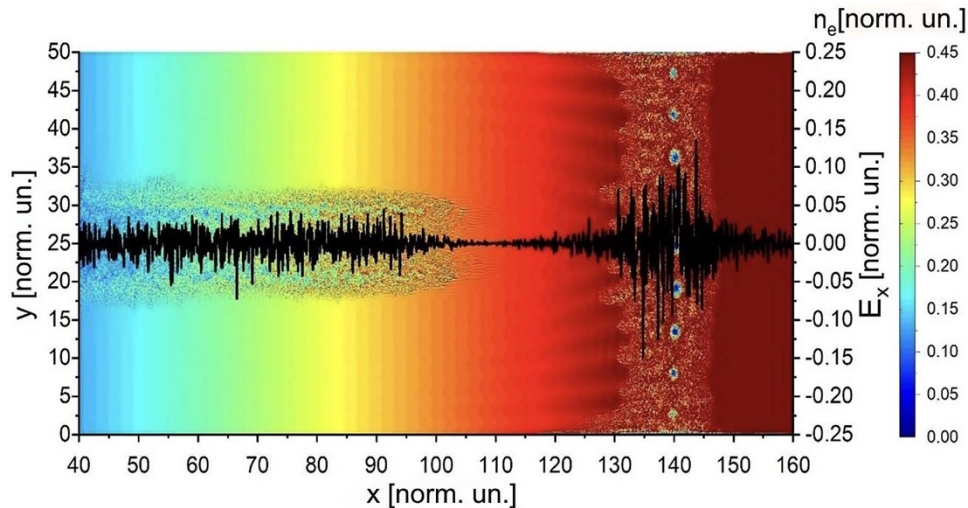$x = x_{cr} = 140$, while $n_e(0, y) = 0$. We can see that a strongly perturbed region is formed in all the range $130 < x < 146$ (i.e. $n_e \lesssim n_{cr}$) and in all cross-section $0 < y < 50$.

Figure 1 shows that the perturbation is much larger than the initial width of the laser pulse ($\approx 1\,\mu m$). Indeed, as it propagates towards the critical density, the beam gradually expands. Its initial width is λ FW HM and $\approx 8\lambda$ at the base, but at $t = 500$ we can see that its width is already about $\approx 20\lambda$. This is because the laser pulse excites perturbations of the plasma electron density in all the interval $n_{cr}/4 < n_e < n_{cr}$. The scattering by these perturbations produces the gradual expansion of laser pulse.

Then approaching the denser region ($x \geq 120$ in Fig. 1), perturbations grow everywhere due to the resonant response of the resonant region to the Gaussian laser pulse front (but the amplitude of perturbations decreases along y going away from the axis). Indeed at $t = 500$, the Gaussian-like leading edge of the laser pulse has reached the critical layer ($x = x_{cr}$). At this time, elongated layers of reduced electron plasma density are formed for $x < x_{cr}$, like a bowed comb of electron density layers (such layers in 2D will correspond to plasma channels in the real 3D physical situation). These layers are surrounded by shafts of increased plasma electron density which act as reflecting mirrors for the electromagnetic waves. Similar plasma mirror in the form of shock has been presented in Fig. 3 of Ref (9).

As seen in Fig. 1, such layers are inclined with respect to the x-axis, which shows the impact of the scattering in the transverse direction near $n_e = n_{cr}$. This leads to a strong expansion of the beam which affects the whole simulated area. At the same time, the electromagnetic wave with lower frequencies of its spectrum can be trapped by channels, penetrating along the channels to the critical point and bringing to the formation of a train (sequence distributed along y) of cavities with trapped laser field at $x \approx x_{cr}$.

From Figs. 1–3, one can also see that the electromagnetic field, penetrating along channels, is trapped, and accumulated in the cavities. Hence, the amplitude of the electromagnetic field is maximum in the cavity, which hosts half wavelength of the electromagnetic wave. We clearly see that the fields are increased in vicinity of the critical density, i.e. for $x \approx x_{cr}$. Two sequences (distributed
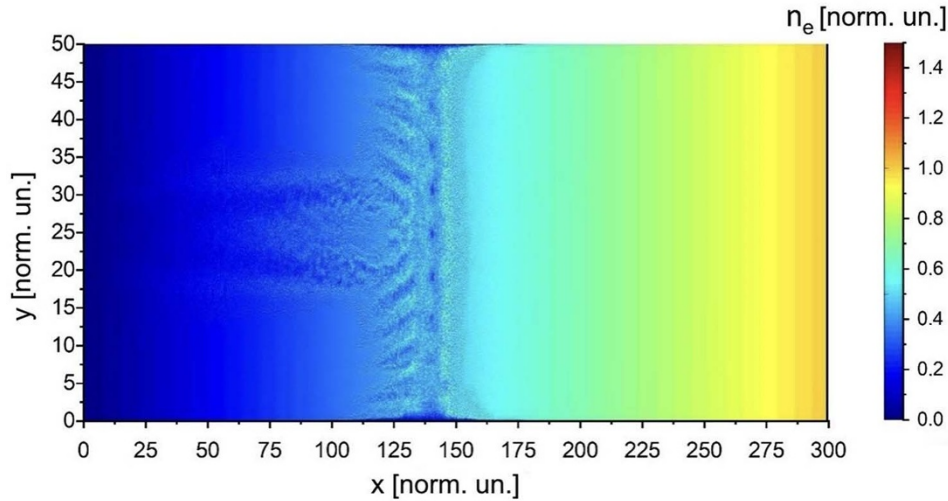
Figure 4. Spatial distribution of plasma electron density $n_e(x, y)$ at time $t = 550$, perturbed by a transversally narrow S-polarized laser pulse.
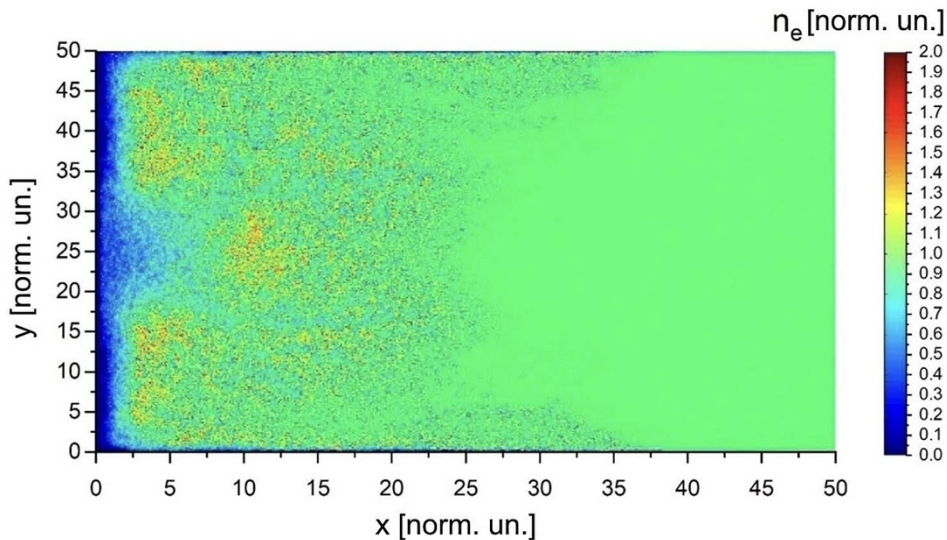

Figure 5. Spatial electron density distribution $n_e(x, y)$ of an initially homogeneous overcritical plasma ($n_e = 2n_{cr}$) perturbed by a transversally narrow Gaussian laser pulse at time $t = 300$. Density is shown in the color bar (remember that here values are normalized to $2n_{cr}$).

along y) of cavities are being formed near the critical point (respectively at $x \approx 137$ and $x \approx 140$, see Fig. 1), the first one of smaller intensity.

Figure 4 shows the situation later ($t = 550$), when the maximum of the laser pulse reached the critical point. We see that the complex channels are spatially separated in Figs. 1–3 from the maximum of the laser pulse while in Fig. 4 they connect with the maximum of the laser pulse. At this later time, it becomes even clearer that the electromagnetic wave can be trapped in the channels penetrating to the critical point along them to the cavities.

To understand the mechanism of channel formation, we simulated the interaction of an S-polarized Gaussian laser pulse (with length 50λ FWHM, width 2λ FWHM, intensity $I \approx 10^{16} W/cm^2$ (14,19), normalized pulse amplitude equals 0.034) with a homogeneous overcritical plasma of density $n_e = 2n_{cr}$ (see Fig. 5).

One can see that the laser pulse forms channels of low density near point of injection. Along these channels, the laser pulse can penetrate deeper into the plasma. Also deeper in the plasma at the end of the channels, the laser pulse forms regions consisting of perturbations of low and high plasma electron density. It should be noted that this numerical simulation was performed in the approximations of immobile and mobile ions. The results are qualitatively close.

Formation of a uniform channel of reduced plasma density for s-polarization

As numerical simulations show, the sequence of cavities distributed along y, shown in Fig. 2, is unstable. At later times (e.g. $t = 600$), this is transformed into a transverse uniform channel in correspondence to the critical layer $x \approx x_{cr}$ (see Fig. 6). Also, from
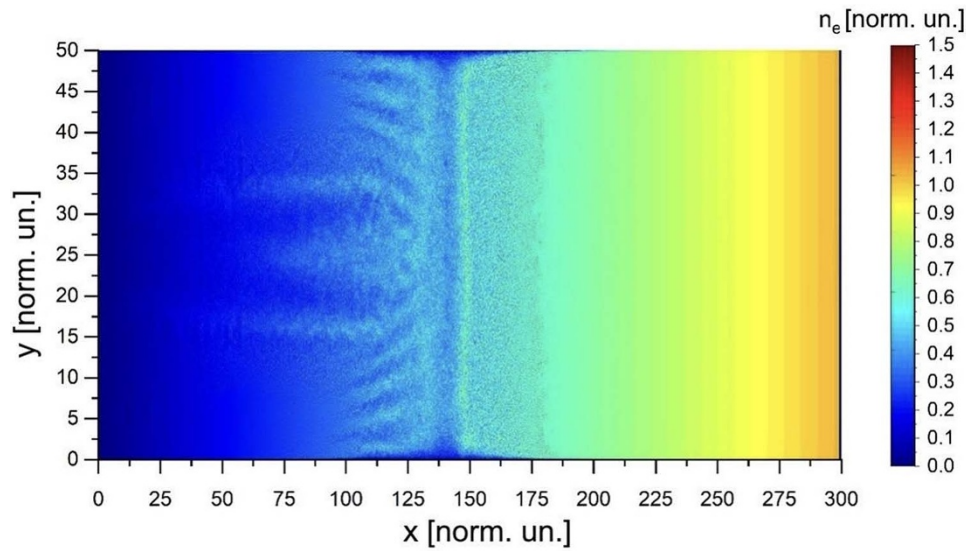
Figure 6. Spatial distribution of plasma electron density $n_e(x, y)$ at time $t = 600$, perturbed by a transversally narrow S-polarized laser pulse.
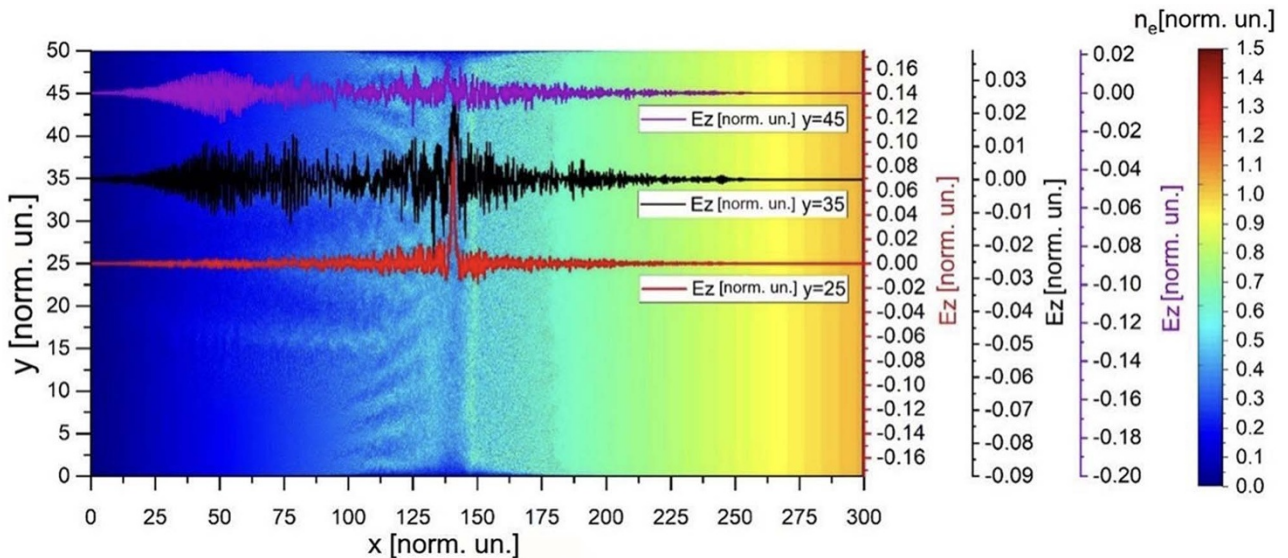

Figure 7. Spatial distribution of plasma electron density $n_e(x, y)$ (shown by color map) and longitudinal distribution of laser field $E_z(x)$ at time $t = 600$ for $y = 25$ (laser injection axis), $y = 35$ and $y = 45$. One can see that in the region $n_e = n_{cr}/4$ electromagnetic pulse has greatly expanded.

the E_z graphs in Fig. 7, one can see that in the channel there is trapped laser field and its amplitude decreases from the laser axis to the transversal boundaries. It can be assumed that the transverse inhomogeneity of the trapped laser field has been sufficient to provide a ponderomotive force able to produce the merging of the cavities into a uniform channel directed in the transverse direction.

One can also see that the fast oscillations of the electromagnetic field trapped in the uniform channel led to the formation of a layer of perturbations in vicinity of the critical layer for $x \gtrsim x_{cr}$.

The scenario shown in Figs. 1–4, 6 and 7 for different times shows that a strongly inhomogeneous distribution of plasma electron density cavities with trapped laser field can be damped and self-consistently produce (at $t = 600$, as shown in Figs. 6 and 7) a uniform plasma density distribution in the transverse direction, under the action of ponderomotive forces (i.e. Miller forces) of adjacent laser pulses, of the trapped in cavities electromagnetic

field, of the scattered field, and under the action of a pressure of heated electrons.

Case of P-polarized laser light

Let's consider now the case of P-polarized laser pulse. From Fig. 8 one can see that up to $t = 400$, a strongly disturbed '*two-petal like*' perturbation is formed for $x < 125$ (i.e. $n_e < n_{cr}$). In the region $n_e = n_{cr}/4$ electromagnetic pulse has already greatly expanded. Figures 9 and 10 show that, at later times, channels of reduced plasma electron density, surrounded by shafts of increased plasma electron density are formed for $x < x_{cr}$ in the case of P-polarized laser pulses, similarly to the S-polarization case.

Simulations show that when the first front of the *two-petal perturbation* reaches the critical density, the nuclei of a uniform channel directed along y begin to develop from the ends of the perturbation towards the axis. Finally, the interaction of the laser
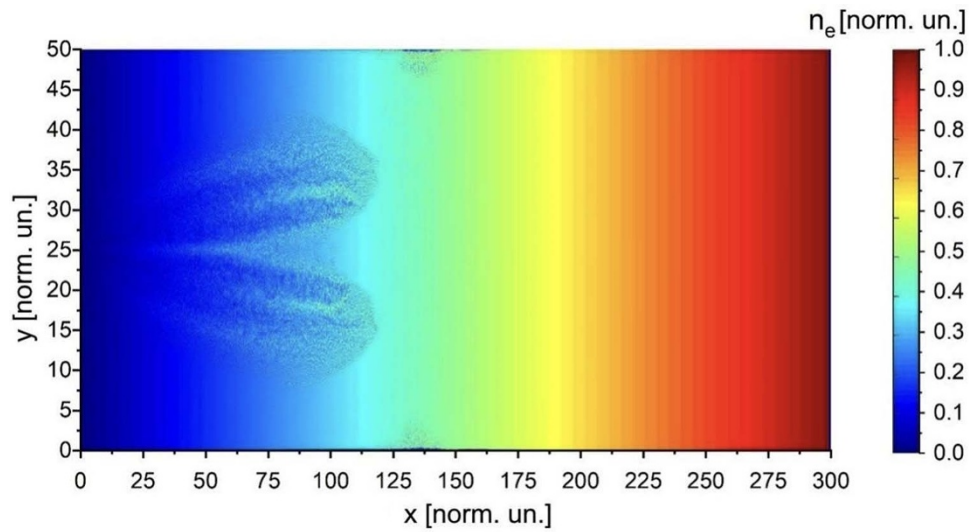
Figure 8. Spatial distribution of plasma electron density $n_e(x, y)$ at time $t = 400$, perturbed by an initially narrow P-polarized laser pulse.
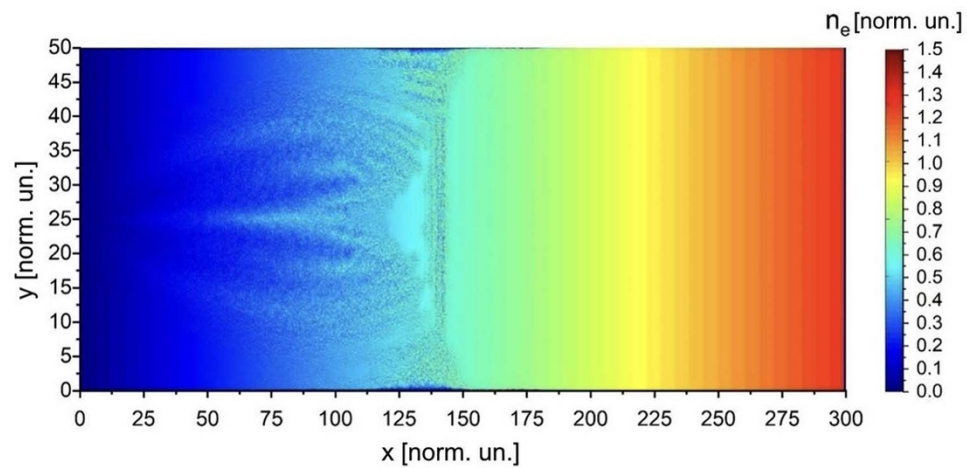

Figure 9. Spatial distribution of plasma electron density $n_e(x, y)$ (shown by colors) at time $t = 450$, perturbed by initially narrow P-polarized laser pulse.

Figure 10. Spatial distribution of plasma electron density $n_e(x, y)$ (shown by colors) at time $t = 500$, perturbed by initially narrow P-polarized laser pulse.
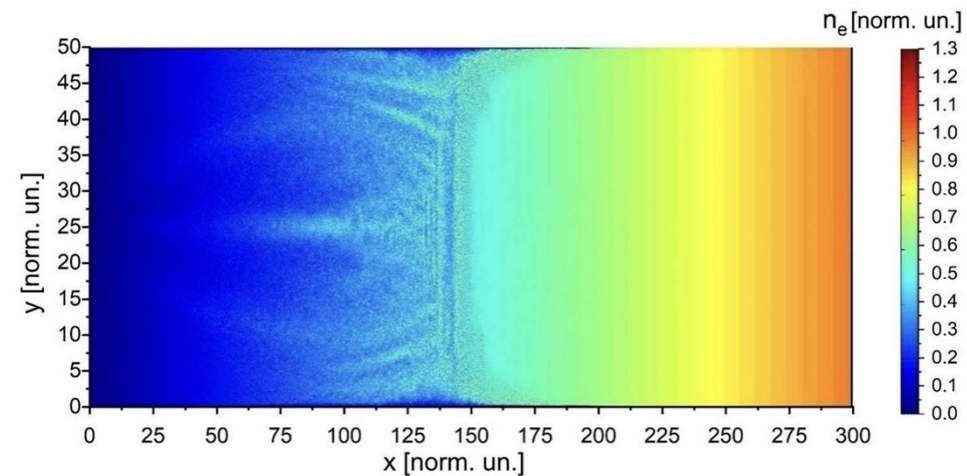
pulse with the dense inhomogeneous plasma produces a uniform transversal channel, via the scattering of a laser pulse in transverse direction (10). Figure 10 shows that by the time $t = 500$, the channel occupies almost the entire cross-section of the simulation box.

It is necessary to note that at the time $t = 450$ (Fig. 9), the laser pulse has not yet reached the critical surface along the axis ($y = 25$) but the laser field from the periphery has already reached the critical layer and begun to form the homogeneous channel directed along y.

One can assume that the formation of the transverse channel and the smoothing of the transverse inhomogeneity is due to the synergetic effect of the combined fields of the adjacent laser pulses, which penetrated to the critical point (see Fig. 8), and due to the synergetic effect of the combined fields of the laser pulse, which penetrated to the critical point (at the ends of two-petal perturbation) along the trapping inclined channels.

Conclusions

We have studied the interaction of transversely narrow S- and P-polarized laser pulses with an inhomogeneous plasma through numerical simulations. The results reveal that regions of reduced electron density form within the plasma, acting as channels that guide the lower-frequency components of the laser pulse toward the critical density layer, while higher-frequency components are transversely scattered. At the critical layer, localized plasma cavities emerge and progressively coalesce into a uniform transverse channel. This process leads to the self-consistent suppression of initial plasma inhomogeneities. These findings are particularly significant for inertial confinement fusion (ICF), where uniform energy deposition in the near-critical density region is crucial for effective energy coupling and target compression.

Future research will aim to refine the model by incorporating finite electron temperature effects and further exploring the influence of high-frequency scattering on the formation and evolution of uniform plasma channels.

References

1. **Hadžievski LJ, Jovanović MS, Škorić MM and Mima K** (2002) Stability of one-dimensional electromagnetic solitons in relativistic laser plasmas. *Physics of Plasmas* **9**(6), 2569–2574. doi:10.1063/1.1476665

2. **Schamel H and Maslov VI** (1994) Adiabatic growth of electron holes in current-carrying plasmas. *Physica Scripta* **T50**, 42–46. doi:10.1088/0031-8949/1994/T50/006

3. **Schamel H and Maslov V** (1999) Langmuir wave contraction caused by electron holes. *Physica Scripta* **T82**(1), 122. doi:10.1238/Physica.Topical.082a00122

4. **Kaw PK, Sen A and Katsouleas T** (1992) Nonlinear 1D laser pulse solitons in a plasma. *Physical Review Letters* **68**(21), 3172–3175. doi:10.1103/PhysRevLett.68.3172

5. **Chandra S, Das C, Kabi J, Batani D, Aliverdiev A, Majumdar A, Ghosal R, Mallick S, Panda B and Sen A** (2024) Evolutionary Stages of Envelope Soliton During Laser Plasma Interaction. *IEEE Transactions on Plasma Science*. doi:10.1109/TPS.2024.3388317

6. **Vu HX, DuBois DF, Russell DA, and Myatt JF** (2012) Hot-electron generation by 'cavitating' Langmuir turbulence in the nonlinear stage of the two-plasmon–decay instability. *Physics of Plasmas* **19**(10), 102708. doi:10.1063/1.4764075

7. **Vu HX, DuBois DF, Russell DA, Myatt JF and Zhang J** (2014) Nonlinear development of the two-plasmon decay instability in three dimensions. *Physics of Plasmas* **21**(4), 042705. doi:10.1063/1.4871717

8. **Li CK, Tikhonchuk V, Moreno Q, Sio H, d'Humieres E, Ribeyre X, Korneev P, Atzeni S, Betti R and Birkel A** (2019) Collisionless shocks driven by supersonic plasma flows with self-generated magnetic fields. *Physical Review Letters* **123**(5), 055002. doi:10.1103/PhysRevLett.123.055002

9. **Tseluyko AF, Lazurik VT, Ryabchikov DL, Maslov VI and Sereda IN** (2008) Experimental study of radiation in the wavelength range 12.2–15.8 nm from a pulsed high-current plasma diode. *Plasma Physics Reports* **34**(11), 963–968. doi:10.1134/S1063780X0811010X

10. **Batani D, Baton S, Casner A, Depierreux S, Hohenberger M, Klimo O, Koenig M, Labaune C, Ribeyre X, Rousseaux C and Schurtz G** (2014) Physics issues for shock ignition. *Nuclear Fusion* **54**(5), 054009. doi:10.1088/0029-5515/54/5/054009

11. **Shang WL, Betti R, Hu S, Woo K, Hao L, Ren C, Christopherson AR and Bose A** (2017) Electron shock ignition of inertial fusion targets. *Physical Review Letters* **119**(19), 195001. doi:10.1103/PhysRevLett.119.195001

12. **Atzeni S, Ribeyre X, Schurtz G, Schmitt AJ, Canaud B, Betti R and Perkins LJ** (2014) Shock ignition of thermonuclear fuel: Principles and modelling. *Nuclear Fusion* **54**(5), 054008. doi:10.1088/0029-5515/54/5/054008

13. **Ribeyre X, Schurtz G, Lafon M, Galera S and Weber S** (2009) Shock ignition: An alternative scheme for HiPER. *Plasma Physics and Controlled Fusion* **51**, 015013. doi:10.1088/0741-3335/51/1/015013

14. **Theobald W, Anderson KS, Betti R, Craxton RS, Delettrez JA, Frenje JA, Glebov VY, Gotchev OV, Kelly JH, Li CK and Mackinnon AJ** (2009) Advanced-ignition-concept exploration on OMEGA. *Plasma Physics and Controlled Fusion* **51**, 124052. doi:10.1088/0741-3335/51/12/124052

15. **Tentori A, Colaïtis A and Batani D** (2022) 3D Monte-Carlo model to study the transport of hot electrons in the context of inertial confinement fusion. Part I. *Matter & Rad at Extremes* **7**, 065902. doi:10.1063/5.0103631

16. **Filippov ED, Khan M, Tentori A, Gajdos P, Martynenko AS, Dudzak R, Koester P, Zeraouli G, Mancelli D, Baffigi F, Gizzi LA, Pikuz SA and Nicolaï PD** (2023) Characterization of hot electrons generated by laser–plasma interaction at shock ignition intensities. *Matter & Rad at Extremes* **8**, 065602. doi:10.1063/5.0157168

17. **Yu C, Tian Y, Li W, Zhang Z, Qi R, Wang W, Wang C and Liu J** (2016) Study of channel formation and relativistic ultra-short laser pulse propagation in helium plasma. *Plasma Physics & Controlled Fusion* **58**(5), 055007. doi:10.1088/0741-3335/58/5/055007

18. **Krushelnick K, Ting A, Moore CI, Burris HR, Esarey E, Sprangle P and Baine M** (1997) Plasma channel formation and guiding during high intensity short pulse laser plasma experiments. *Physical Review Letters* **78**(21), 4047–4050. doi:10.1103/PhysRevLett.78.4047

19. **Freeman RR, Batani D, Baton S, Key M and Stephens R**. (2006) The generation and transport of large currents in dense materials: The physics of electron transport relative to fast ignition. *Fusion Science and Technology* **49**, 297. doi:10.13182/FST06-A1150